Acta Geochim
https://doi.org/10.1007/s11631-024-00727-w

ORIGINAL ARTICLE

Geology and S-Pb isotope geochemistry of the Hatu gold deposit in West Junggar, NW China: Insights into ore genesis and metal source

Shen Han[1] · Zhenju Zhou[2,3,4] · Xiaohua Deng[5] · Yanshuang Wu[6] · Xi Chen[7] · Abulimiti Aibai[6] · Yong Wang[8] · Xiaoyu Jia[1] · Yanjing Chen[1,6,9]

Received: 22 April 2024 / Revised: 21 June 2024 / Accepted: 29 July 2024

Abstract The Hatu gold deposit is the largest historical gold producer of the West Junggar, western China, with an Au reserve of about 62 t. The orebodies were controlled by NE-, EW-, and NW-trending subsidiary faults associated with the Anqi fault. This deposit exhibits characteristics typical of a fault-controlled lode system, and the orebodies consist of auriferous quartz veins and altered wall rocks within Early Carboniferous volcano-sedimentary rocks. Three stages of mineralization have been identified in the Hatu gold deposit: the early pyrite-albite-quartz stage, the middle polymetallic sulfides-ankerite-quartz stage, and late quartz-calcite stage. The sulfur isotopic values of pyrite and arsenopyrite vary in a narrow range from −0.8‰ to 1.3‰ and an average of 0.4‰, the near-zero $\delta^{34}S$ values implicate the thorough homogenization of the sulfur isotopes during the metamorphic dehydration of the Early Carboniferous volcano-sedimentary rocks. Lead isotopic results of pyrite and arsenopyrite ($^{206}Pb/^{204}Pb = 17.889$–$18.447$, $^{207}Pb/^{204}Pb = 15.492$–$15.571$, $^{208}Pb/^{204}Pb = 37.802$–$38.113$) are clustered between orogenic and mantle/upper crust lines, indicating that the lead was mainly sourced from the hostrocks within the Early Carboniferous Tailegula Formation. The characteristics of S and Pb isotopes suggest that the ore-forming metals of the Hatu orogenic gold deposit are of metamorphogenic origin, associated with the continental collision between the Yili-Kazakhstan and Siberian plates during the Late Carboniferous.

Keywords Hatu gold deposit · Sulfur isotope · Lead isotope · Orogenic gold deposit · West Junggar

Supplementary Information The online version contains supplementary material available at https://doi.org/10.1007/s11631-024-00727-w.

✉ Zhenju Zhou
zhenjuzhou@126.com

✉ Yanjing Chen
gigyjchen@126.com; yjchen@pku.edu.cn

1 Key Laboratory of Orogenic Belts and Crustal Evolution of Ministry of Education, Peking University, Beijing 100871, China

2 Institute of Geomechanics, Chinese Academic of Geological Science, Beijing 100081, China

3 Key Laboratory of Paleomagnetism and Tectonic Reconstruction of Ministry of Natural Resources, Beijing 100081, China

4 Radiogenic Isotope Facility, School of Earth and Environmental Sciences, The University of Queensland, Brisbane 4072, Australia

5 Key Laboratory of Western China's Mineral Resources and Geological Engineering, Ministry of Education, School of Earth Science and Resources, Chang'an University, Xi'an 710054, China

6 Xinjiang Mineral Resources Research Center, Xinjiang Institute of Ecology and Geography, Chinese Academy of Sciences, Urumqi 830011, China

7 Guangdong Provincial Key Lab of Geodynamic and Geohazards, School of Earth Sciences and Geological Engineering, Sun Yat-Sen University, Guangzhou 510275, China

8 Western Region Gold Co., Ltd., Urumqi 830002, China

9 The National 305 Project Office of the People's Government of Xinjiang Uygur Autonomous Region, Urumqi 830000, China

Published online: 21 August 2024

1 Introduction

In the West Junggar, western China, more than 200 gold deposits have been identified, with estimated reserves of over 100 t (Shen and Jin 1993). The Hatu gold deposit, with an Au reserve of 62 t and average grade of 5 g Au/t, is considered to be one of the most representative gold deposits in this region. The orebody is hosted in Early Carboniferous volcano-sedimentary rocks (Fan et al. 1998; Xiao et al. 2010b). There are still some disputes about the ore genesis of the Hatu gold deposit. Some researchers have classified the deposit as intrusion-related deposit, exclusively attributed to the magmatic hydrothermal processes during the Late Paleozoic, based simply on the temporal and spatial associations, as well as the similar stable isotopic ratios with granitoids (Zhu et al. 2013; Wang and Zhu 2015; Wang et al. 2019a, b; An et al. 2023). Shen et al. (2016) suggested that in addition to the involvement of magmatic fluids, the mineralization in Hatu gold deposit incorporates the contribution of mantle-derived fluids. However, other studies favor the fact that the Hatu gold deposit recognized as orogenic-type are the consequences of crustal metamorphic processes, specifically formed during the continental collision regime in the Late Carboniferous-Permian (Permo-Carboniferous) (Chen and Zhang 1991; Chen 1996; Ding et al. 2019; Zheng et al. 2022).

To clarify the ore genesis and ore-forming mechanism of the Hatu deposit, we revisit the ore geology and ore-forming conditions, and conclude that the deposit is a typical fault-controlled lode system formed during post-subduction collisional orogenesis, i.e. orogenic-type gold deposit. We also summarize available the sulfur and lead isotope data, including those obtained by the authors, and thereby, determine the source of ore-forming fluids and metals (Richards and Kerrich 1993; Chen et al. 2004a, b; Hodkiewicz et al. 2009). Finally, we propose a genetic model of orogenic-type gold mineralization in West Junggar and adjacent areas.

2 Regional geology

The Central Asian Orogenic Belt (CAOB), also referred to as the Altaid tectonic collage or Central Asian Orogenic System (Fig. 1a), represents a significant Phanerozoic orogenic belt and has experienced a complex history of orogenic development, characterized by multiple stages of orogenic development including continental accretion, post-collisional events, and intracontinental orogeny (Khain et al. 2002; Kröner et al. 2007; Xiao and Kusky 2009; Choulet et al. 2011, 2012; Pirajno et al. 2011). It preserves the geological evidence of the Paleo-Asian Ocean's closure (Coleman 1989; Şengör et al. 1993; Şengör and Natal'In 1996; Xiao et al. 2010a; Hong and Liu 2021). The Early Paleozoic southwestern Paleo Asian Ocean (PAO) was composed of four branches: Irtysh-Zaysan Ocean, Junggar-Balkhash Ocean, Uralian Ocean, and Turkestan Ocean (Filippova et al. 2002), and the former two played a significant role in the evolution of West Junggar Orogenic Belt. The CAOB occupies the region between the Siberian Craton to the north and the North China and Tarim Cratons to the south (Xiao et al. 2003; Buckman and Aitchison 2004; Windley et al. 2007; Kröner et al. 2014).

The West Junggar is situated within the central part of the CAOB, bordered by the Altai Orogen to the north, the Tianshan Orogen to the south, and the Junggar Basin to the east (Fig. 1b). Present-day West Junggar has undergone a complicated and protracted geological evolution as oceanic crust has been subducted and arcs accreted since the Late Neoproterozoic (Xiao et al. 2008). Based on their unique geological features and evolutionary history, three major lithotectonic units can be recognized in this region: southern, central, and northern West Junggar (Xu et al. 2013). Among them, the central West Junggar features the occurrence of volcano-sedimentary rock successions from the Early Carboniferous, which can be classically divided into Xibeikulasi, Baogutu, and Tailegula Formations from bottom to the top. The Xibeikulasi Formation comprises tuffaceous conglomerate, greywacke, and lithic tuff, and the overlying Baogutu Formation comprises tuffaceous siltstone and tuff (Guo et al. 2010; Shen et al. 2016). The Tailegula Formation consists of Carbonaceous mudstone, siltstone, gray-green tuff, basalt, and jasper (Wang and Zhu 2007).

Prior to the Late Carboniferous, two distinct episodes of plutonism are recognized in the West Junggar and are spatially and temporally separated (Zheng et al. 2019), between ca.533–485 and 445–321 Ma (Zheng et al. 2019; Ren et al. 2014; Xu et al. 2012; Chen et al. 2019). Plutons of the older period are exclusively found within the southern West Junggar, appearing as small and isolated bodies, and these deformed plutons have been fragmented and involved into the Ordovician to Devonian accretionary complexes (Zheng et al. 2019) and demonstrate discernible enrichment in LREE and LILE, along with a depletion in HFSE (Xu et al. 2013; Zheng et al. 2019; Liao et al. 2021). The oldest is recorded by the Kekesayi pluton, which comprises two distinct age groups of 579–500 Ma and the older group of zircon grains yielded a U–Pb weighted mean age of 572 ± 4 Ma (Zheng et al. 2019). Plutons from the younger period are commonly located in the northern West Junggar, absolute age estimates for this episode have it beginning at approximately ~445 Ma and ending at ~320 Ma, and mainly involves the Zharma-Saur and Boshchekul-Chingiz arc (Li et al. 2017; Liu et al. 2018).

Subsequent to the Late Carboniferous, the West Junggar developed pronounced occurrence of anorogenic (A)-type granitoid intrusions that contain alkaline granite, alkali feldspar granite, and monzogranite (Chen and Jahn 2004). These

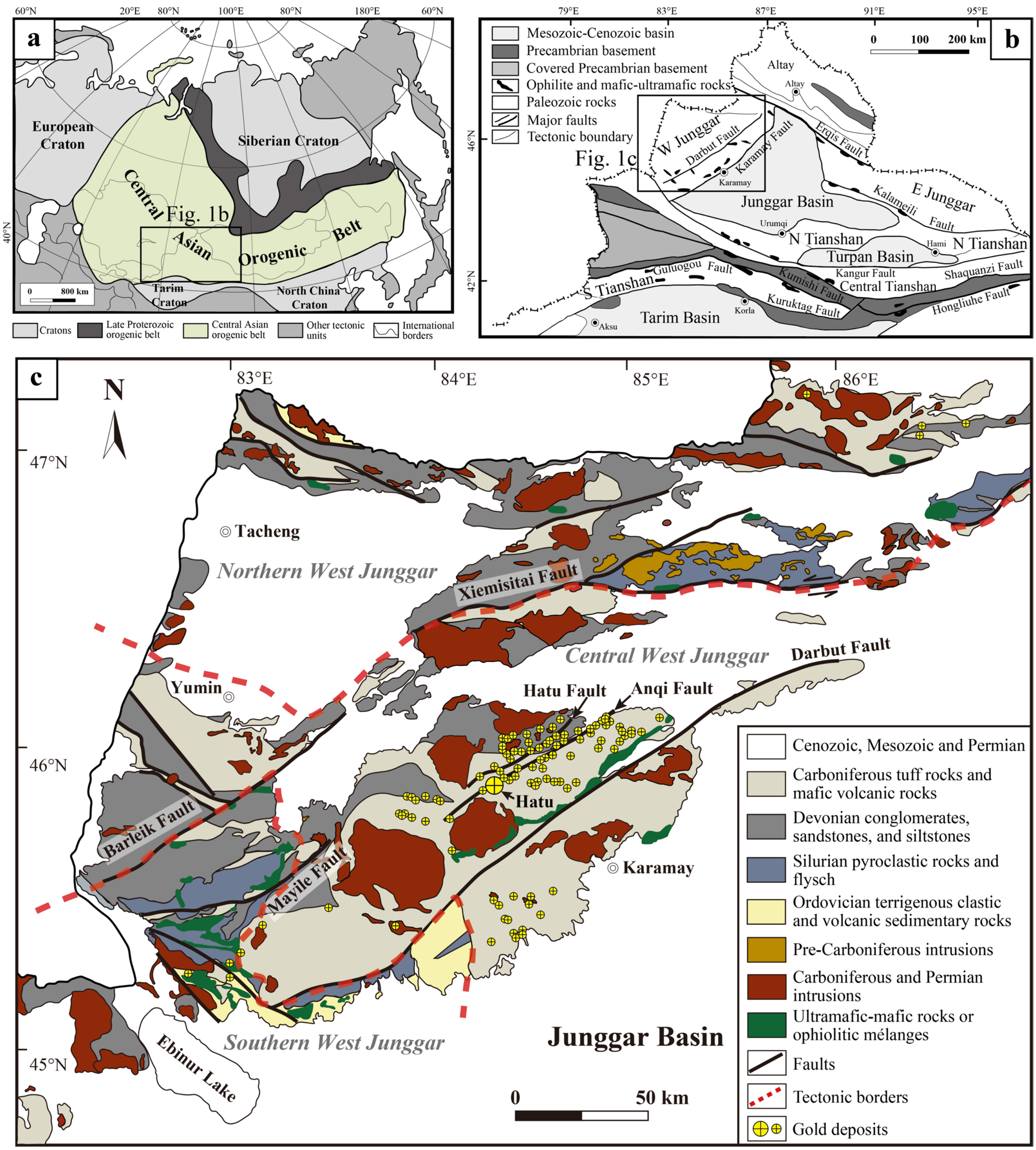

Fig. 1 Tectonic locations of West Junggar and the Hatu gold deposit. **a** Simplified geological map of the Central Asian Orogenic Belt (modified after Xiao et al. 2008); **b** Simplified geological map illustrating tectonic units in North Xinjiang (modified after Chen et al. 2012a); **c** Regional geological map of West Junggar showing the location and geological setting of Hatu gold deposit (modified after Xu et al. 2012)

include the Hatu alkali feldspar granite (305 ± 4 Ma, Gao et al. 2014), Karamay monzogranite (304 ± 5 Ma, Yang et al. 2014), Akebasitao granite (290 ± 8 Ma, Han et al. 2006; 316 ± 2 Ma, Li et al. 2016), and Miaoergou alkali feldspar granite (309 ± 1 Ma, Hu et al. 2015). These granite plutons signify a remarkable vertical crustal growth during the Late Paleozoic and suggests a post-collisional setting throughout

West Junggar (Han et al. 1997, 2006; Xu et al. 2012; Chen et al. 2015; Liu et al. 2019).

Left-lateral strike-slip faults of Darbut, Mayile, and Baerleike outline the domino-type tectonic system (Feng et al. 1989; Chen et al. 2011; Lin et al. 2017). The southern West Junggar terrane comprises successive island arc and accretionary complexes separated by northeast trending faults (Li et al. 2014), while the northern West Junggar terrane is characterized by east–west trending faults (Yang et al. 2020). In the central West Junggar, the prominent sinistral transform Darbut fault, extending over 200 km in length and reaching depths exceeding 6 km), has experienced substantial nonferrous metal mineralization on its northern side (Yang et al. 2012). Subordinate northeast trending faults such as the Anqi and Hatu faults generally control the formation and distribution of ore deposits in Hatu gold mining district (Fig. 1c).

3 Deposit geology

The Hatu gold mining district is situated on the south slope of Mount Hatu near the Darbut fault and hosts gold deposits such as Hatu, Qi-II, Qi-III, Qi-IV, Qi-V, Gezigou, and Mandongshan (Fig. 1c). The strata exposed in Hatu gold deposit is the Early Carboniferous Tailegula Formation, which is composed of a succession of basalt and tuff interbedded with tuffaceous siltstone and jasper rocks (Fig. 2; WRGKHGD Co., Ltd. 2018). LA-ICP-MS zircon U-Pb analysis indicates ages of 315 ± 4 and 328 ± 2 Ma for the basalt and tuff, respectively (Wang and Zhu 2007; Tang et al. 2012). Zhu et al. (2013) reported that unaltered diabase dikes, which are attributed to post-mineralization magmatic activity, have yielded zircon U–Pb age of 295.4 ± 4.6 Ma, providing a minimum age for gold mineralization.

Structural deformation, including faults and folds, is widespread within the Hatu gold deposit (Fig. 3), with orebodies predominantly hosted in east–west and/or northwest trending subsidiary faults and fractures that are correlated with the Anqi fault (Fig. 2b). The Anqi fault represents ductile shear deformation mainly involving mylonitized volcanic-sedimentary rocks from the Tailegula Formation with mylonitic fabric and alteration, indicating a greenschist and sub-greenschist facies metamorphic condition during the ductile deformation (Shen et al. 2016). Kinematic indicators, such as composite planar (S-C) fabrics defined by quartz and arsenopyrite, suggest a top to the right shear sense (Fig. 3d, e), and vertical folds indicate that near NNE trending compression occurred in the deposit (Fig. 3a).

Nearly a hundred individual orebodies have been identified in the Hatu gold deposit (Shen et al. 2010; WRGKHGD Co. Ltd., 2018). Individual orebodies typically exhibit a range in grade from 4.3 to 16.6 g Au/t, with some reaching up to 300 g Au/t (Zhang 2003). Orebody L27-8, the dominant industrial concealed orebody, strikes northeast or west–east (Fig. 2c), spanning a strike length of 800 m, with an average thickness of 4.23 m, and a depth of 1046 m (WRGKHGD Co., Ltd. 2018). The hydrothermal veins also display the occurrence of balk reappearence and compound branches (Fig. 2c), presenting as the form of stratiform and lenses with variable degrees of wall rock alteration (Fig. 4; Xiao et al. 2010b). The primary gangue minerals consist of quartz, calcite, albite, muscovite, sericite, chlorite, apatite, and ankerite, while the dominant ore minerals comprise pyrite and arsenopyrite, accompanied by minor amounts of chalcopyrite, native gold, sphalerite, tetrahedrite, electrum, cobaltite, and bournonite. The gold mineralization is closely associated with silicification, pyritization, and arsenopyritization (Fig. 4).

Based on the fieldwork, petrographic observations, crosscutting relationships, and their microscopy characteristics, the mineralization process of the Hatu gold deposit can be divided into three distinct stages, early, middle, and late (Fig. 5). The pyrite-albite-quartz stage (early-stage) is indicated by coarse-grained milky quartz veins (Q1) containing coarse-grained albite, euhedral pyrite (Py1), and some arsenopyrite (Apy1) (Fig. 5a, h). Py1 grains are mainly cubic and pyritohedron ranging in size from 0.3 to 2 mm (Fig. 5d), whereas Apy1 grains are mostly occurred as arsenopyrite twin crystal with sizes ranging from 0.2 to 2 mm (Fig. 5f). Unaltered or deformed Py1 shows oscillatory growth zoning, indicative of changing fluid composition in a stable environment (Fig. 6). The barren milky quartz veins, ranging from a few centimeters to a few meters in thickness, commonly suggest deformation including asymmetric folds and S-C fabrics such as arsenopyrite fish (Fig. 3e, g), and book-inclined features, indicating a compressional setting. The polymetallic sulfides-ankerite-quartz stage (middle-stage) is identified by veinlets that are < 1–3 mm thick (Fig. 5g). Gold was mainly produced in this stage in the form of inclusions or fissure fillings in middle-stage quartz (Q2), arsenopyrite (Apy2), pyrite (Py2), chalcopyrite, sphalerite, pyrrhotite (Fig. 5i, j). Py2 and Apy2 are anhedral to euhedral, and they form grains with sizes ranging from hundreds to tens of microns (Fig. 5h, j). The absence of deformed textures in the middle-stage minerals indicates their formation in a tensile shear setting. The quartz-calcite stage (late stage) is characterized by the deposition of barren quartz-calcite veins crosscutting the earlier formed hydrothermal veins, minerals, and wall rocks (Fig. 5c, l). In these veinlets, transparent and euhedral quartz crystals (Q3) grew toward vugs that were subsequently filled by calcite, implying the calcite precipitated somewhat later than the quartz. Additionally, no pyrite or other sulfides are observed in this stage, and geodes can be noted in certain late-stage veins (Fig. 5k). The mineral paragenesis sequence is given in Fig. 7.

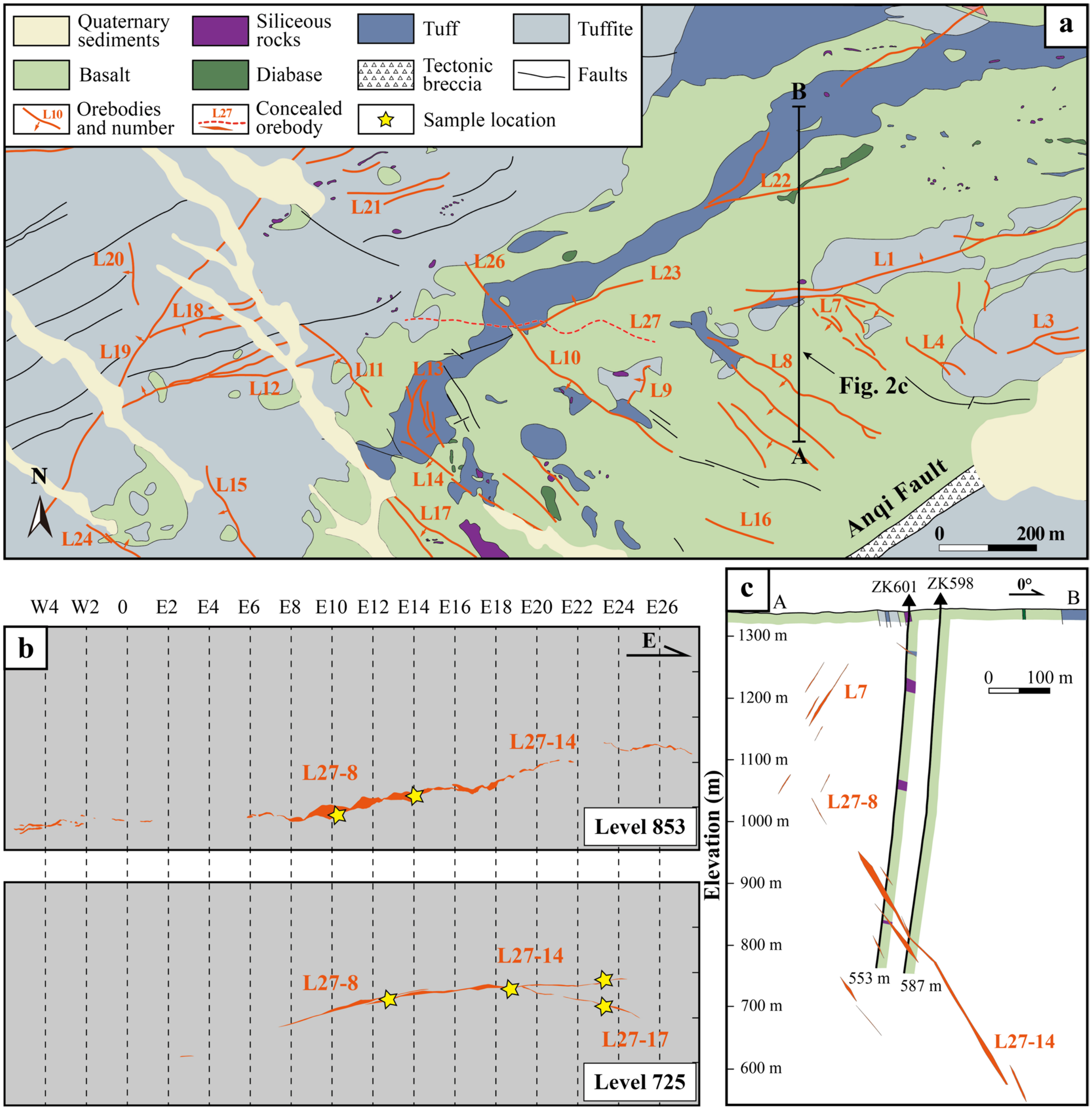

Fig. 2 **a** Geological map of the Hatu gold deposit (modified from WRGKHGD Co. Ltd. 2018) illustrating the distribution of the main orebodies; **b** Exploration levels depicting the orebody geology of the Hatu gold deposit; **c** Selective exploration profile of the Hatu gold deposit showing the occurrence of gold orebodies (modified from WRGKHGD Co., Ltd. 2018)

4 Isotope analytics and results

Samples representing all three mineralization stages were collected from orebodies L27-8, L27-17, and L27-14 at level 725 [699 m below the current ground surface (b.g.s)] and level 853 (557 m b.g.s) (Fig. 2b).

4.1 Sulfur isotope

Samples for sulfur and lead isotope analyses were collected from the quartz veins and altered rocks. Sulfide minerals were handpicked after conventional processing techniques including crushing, oscillation, and heavy liquid and

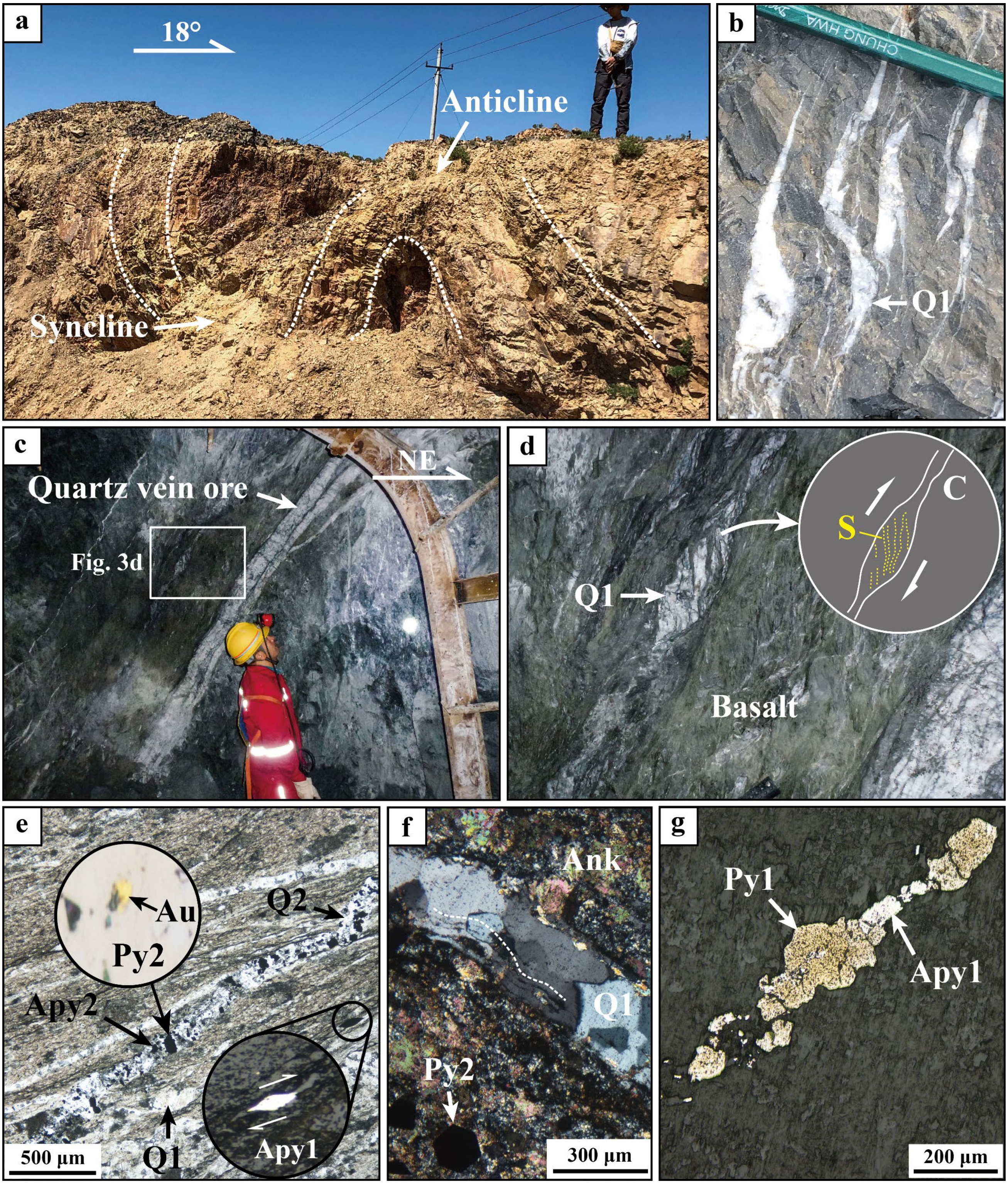

Fig. 3 Photographs from the Hatu gold deposit showing **a** Vertical folds in tuffaceous sandstone; **b** A parallel set of en echelon quartz veins in tuffite, with pencil for scale; **c** An auriferous quartz vein exhibits an elongated slab shape with crack-seal structures; **d** S-C fabric showing right-lateral shearing with strongly foliated altered basalt; the early-stage milky, barren Q1 vein crosscut and dislocated by middle-stage gray, auriferous quartz-sulfide veinlets; **e** Sheared and altered wall rock, showing foliation defined by early-stage quartz and tuffaceous materials; middle-stage polymetallic sulfides and quartz are observed in veinlet that cuts the foliation; arsenopyrite fish showing right-lateral sheared sense; **f** Deformed Q1 vein with Py2 disseminated in the adjacent silicified and carbonated wall rocks; **g** The early-stage pyrite and arsenopyrite are fragmented and exhibit evidence of directional stretching. Q, quartz; Au, native gold; Py, pyrite; Apy, arsenopyrite

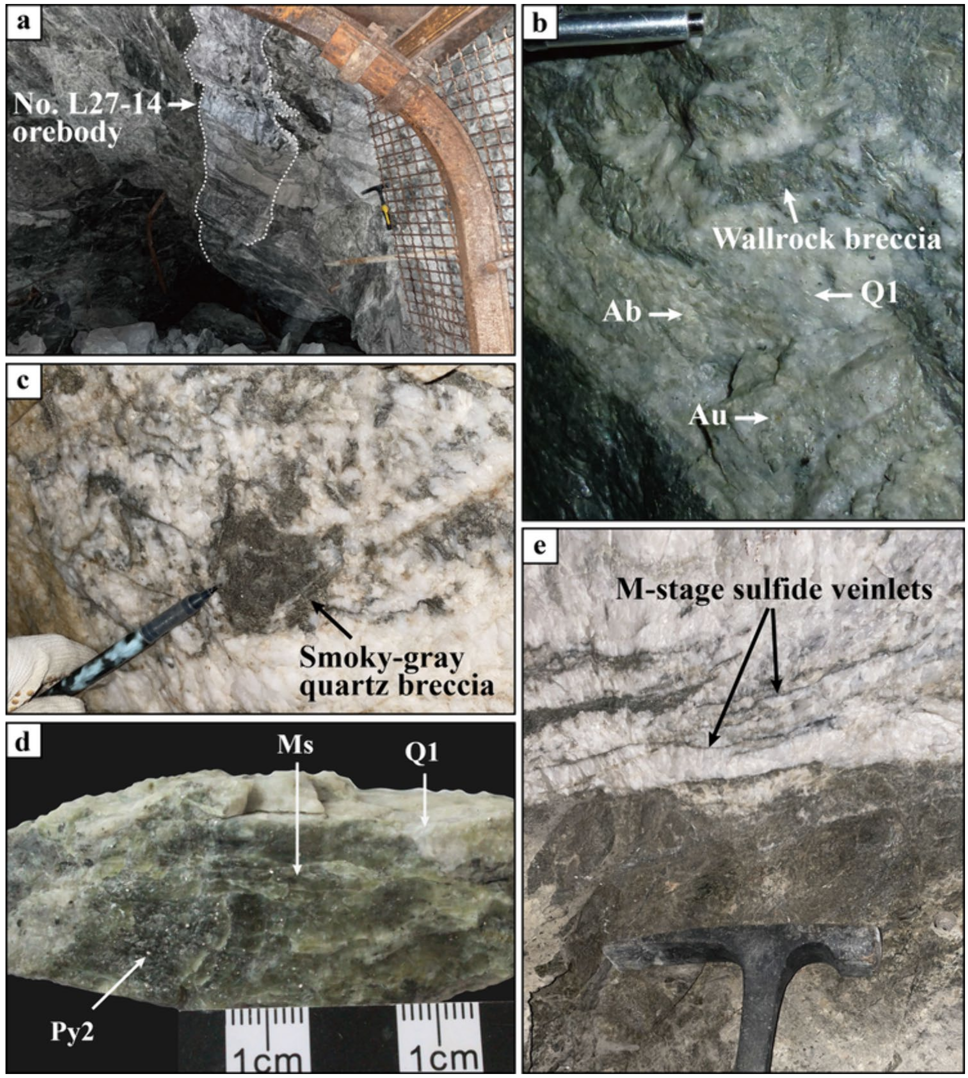

Fig. 4 Orebody characteristics of Hatu gold deposit. **a** L27-14 orebody in the 725 level (599 m b.g.s); **b** Auriferous albite-quartz vein containing altered wallrock breccias; **c** Smoky-gray quartz breccia within milky-white quartz vein; **d** Muscovite flakes in milky quartz; **e** Discontinuous sulfide veinlets that are subparallel to the host rock wall. Q, quartz; Ab, albite; Ms, muscovite; Au, native gold; Py, pyrite

magnetic separation. All separated minerals were further purified by handpicking under a microscope to at least 99% purity. For sulfur isotope analysis, FeS_2 and FeAsS were converted to SO_2 by the vanadium pentoxide (V_2O_5) method. Then, the SO_2 was purified and collected for analysis of the isotopic composition using a Delta v Plus gas isotope ratio mass spectrometer at the Analytical Laboratory of the Beijing Research Institute of Uranium Geology, China. Sulfur isotope values were reported according to the standard $\delta^{34}S$ notation of per mille (‰) relative to Vienna Canyon Diablo Troilite (V-CDT) with an analytical uncertainty (2σ) of ± 0.2‰.

Fifteen samples of ore-bearing sulfides were obtained from the Hatu gold deposit with $\delta^{34}S$ values of − 0.8‰–1.3‰ and an average of 0.4‰ (Table S1). The $\delta^{34}S$ values of the pyrite and arsenopyrite samples had very narrow ranges and were generally close to zero. The five pyrite samples had $\delta^{34}S$ values of − 0.8‰–1.0‰, and the 10 arsenopyrite samples had $\delta^{34}S$ values of − 0.7‰–1.3‰.

4.2 Lead isotope

The lead isotopic composition was measured by using a Phoenix thermal ionization mass spectrometer at the Analytical Laboratory of the Beijing Research Institute of Uranium Geology, China. All lead ratios were calibrated according to the values of the NBS 981 standard. For analysis, samples were dissolved by using HF and $HClO_4$ in crucibles, which was followed by basic anion exchange resin to purify the lead. The external reproducibility of the lead ratios was 0.2% for $^{206}Pb/^{204}Pb$, 0.2% for $^{207}Pb/^{204}Pb$, and 0.6% for $^{208}Pb/^{204}Pb$ at the 2σ level.

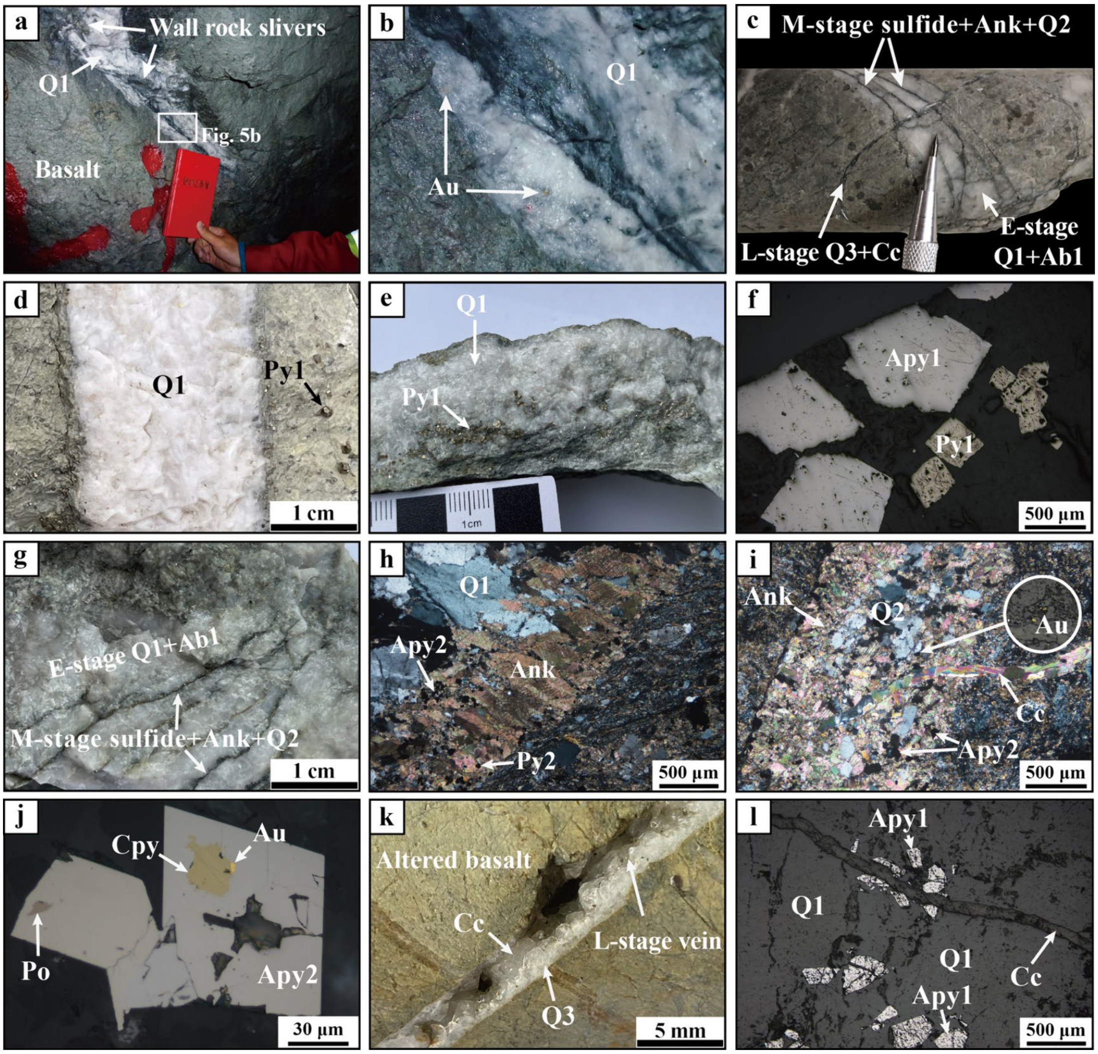

Fig. 5 Photographs showing characteristics and cross-cutting relationships of hydrothermal veins from different mineralization stages in the Hatu gold deposit. **a** Quartz vein ore in altered basalt enclosing irregular wall slivers; **b** Native gold occurs as individual grains in quartz vein; **c** One representative specimen displays cross-cutting relationships of all three-stage veins. The early-stage quartz-albite vein was intersected by middle-stage sulfide-ankerite-quartz veinlets, and then the quartz-calcite vein of late-stage cross-cut both early and middle stage veins; **d** The early-stage barren quartz vein with coarse and pyritohedron pyrite in the adjacent wall rocks; **e** Coarse Py1 developed in the Q1 vein; **f** Coexistence of euhedral Apy1 and Py1 in reflected light; **g** Fractured quartz vein crosscut by middle-stage sulfide-ankerite-quartz veinlets; **h** Disseminated Apy2 and Py2 coexist with comb-textured ankerite, deformed Q1 shows deformation lamellae and sweeping undulose extinction; **i** The calcite vein of late-stage cross-cut the middle-stage vein; **j** Coexisting middle-stage Apy2, Po, and Cpy containing intergranular native gold; **k** The late-stage quartz crystals grew in cavities, later filled by calcite crystals formed in extensional tectonic setting; **l** The early-stage Apy1 was crosscut by the late-stage calcite vein. Q, quartz; Py, pyrite; Apy, arsenopyrite; Cc, calcite; Ank, ankerite; Cpy, chalcopyrite; Po, pyrrhotite; Au, native gold

The measured isotopic composition of lead was compared with previously published data (Table S2) (Shen and Jin 1993; Zheng et al. 2007; Huang 2015; Weng et al. 2020; Zhi et al. 2021). The sulfides from the Hatu gold deposit had $^{206}Pb/^{204}Pb$, $^{207}Pb/^{204}Pb$, and $^{208}Pb/^{204}Pb$ ranges of 17.889–18.447, 15.492–15.571, and 37.802–38.113, respectively, and averages of 17.996, 15.529, and 37.905, respectively. These similar results suggest that the lead isotopic composition was relatively consistent and that these sulfides may have derived from the same source.

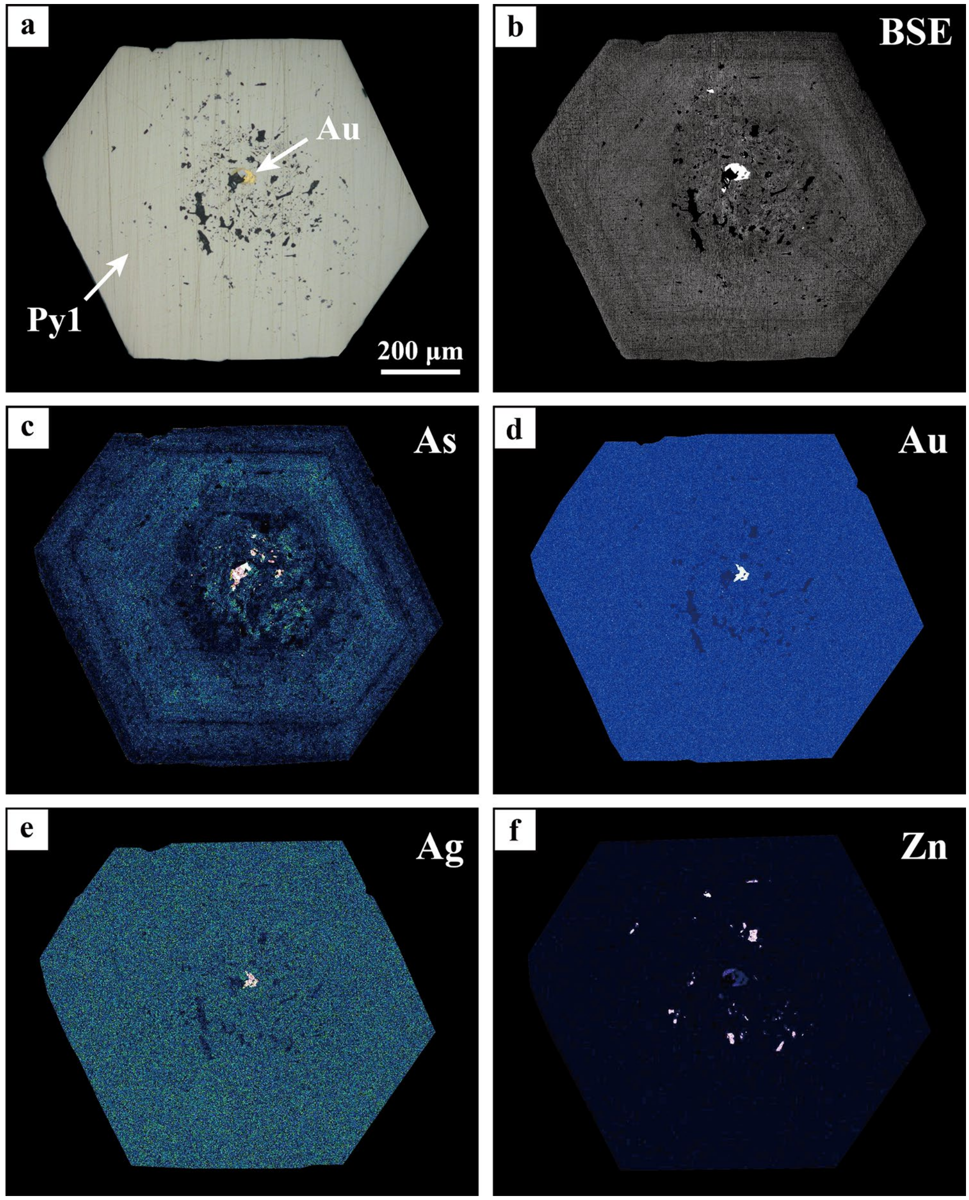

Fig. 6 Backscattered electron image and corresponding qualitative element maps were obtained using energy dispersive spectroscopy mapping on a scanning electron microscope, illustrating compositional variations in Py1. **a** The core of euhedral Py1 contains native gold; **b** Backscattered electron image exhibits oscillatory growth zoning; **c** Bright zones in backscattered electron image correspond to high As contents; **d**, **e** The Py1 contains comparably low Au and Ag concentrations; **f** The occurrence of sphalerite inclusions in Py1

5 Discussion

5.1 Sulfur and lead isotopic compositions and their geological implications

Different sulfides are the primary resource for various metals and sulfur isotope data can be used to effectively constrain the origin of the ore-forming fluid and reveal the gold deposition conditions. The sulfur isotopic composition of sulfides in hydrothermal deposits is determined by the sulfur isotopic composition of the ore-forming fluid as well as the temperature, oxidation–reduction potential (Eh), and pH at the location of mineralization (Ohmoto 1972; Kovalenko et al. 2004; Seal 2006). Whereas the first parameter refers to the source, the others relate to the physicochemical conditions for deposition. The sulfur isotopic compositions of orogenic gold deposits are highly variable. Hodkiewicz et al. (2009) showed that the $\delta^{34}S$ values of hydrothermal pyrite from orogenic gold deposits of the Eastern Goldfields Province in the Yilgarn Craton had a wide range of − 10‰–12‰. When orogenic gold deposits have a wide range of $\delta^{34}S$ values, this can result in puzzling interpretations (LaFlamme et al. 2018). However, a relatively tight clustering of $\delta^{34}S$ values is generally interpreted to indicate that the sulfur source was isotopically uniform (Kishida and Kerrich 1987).

The sulfur isotopic composition of pyrite and arsenopyrite at the Hatu gold deposit had a relatively limited range of − 0.8‰–1.3‰ (Table S1). The near-zero $\delta^{34}S$ values of gold-related sulfides from the Hatu gold deposit overlap with those of most lode gold deposits such as Sawayaerdun (Chen

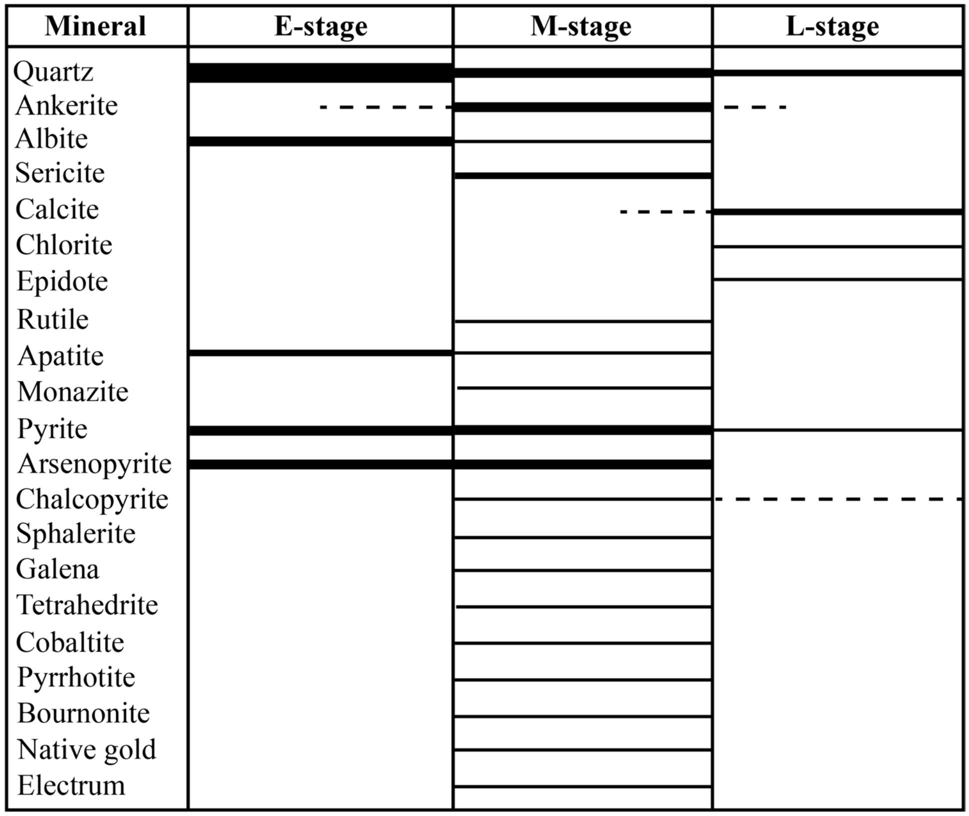

Fig. 7 Paragenesis of hydrothermal minerals in the Hatu gold deposit

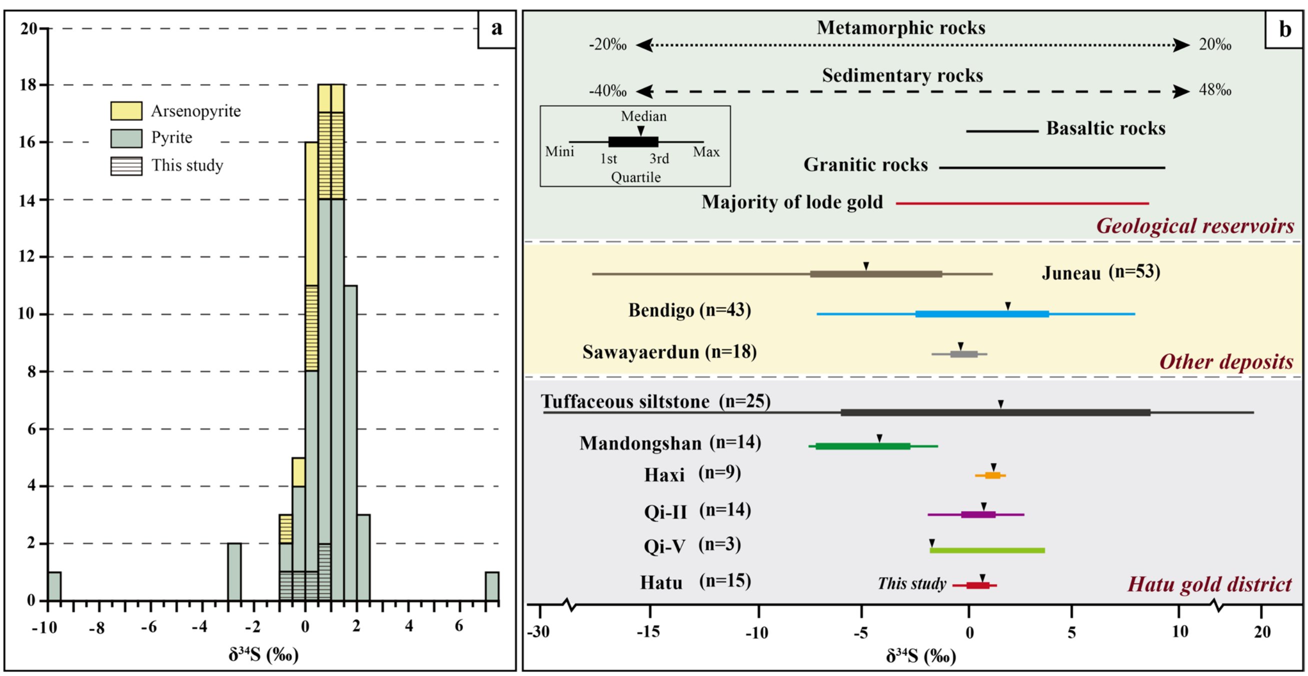

Fig. 8 **a** Histogram illustrating the sulfur isotope composition of sulfides from this study, alongside data previously published for the Hatu gold deposit; **b** Summary of the $\delta^{34}S$ values of sulfides from the Hatu gold mining district, as well as the sulfur isotope composition of various terrestrial reservoirs. References for the ranges of major sulfur deposits and other deposits are given in the text

et al. 2012b), Juneau (Goldfarb et al. 1991), and Bendigo (Jia et al. 2001) for which the ore-forming fluid was concluded to be metamorphic in origin (Phillips and Powell 2010). However, sulfides $\delta^{34}S$ values at Hatu also indicate a comparatively homogeneous magmatic origin (Fig. 8b), as well as the possibility of basalt cannot be precluded. Directly comparing $\delta^{34}S$ values with those of geological reservoirs appears insufficient for accurately ascertaining their source, but they do provide a remarkable amount of information.

The tight unimodal distribution of sulfides $\delta^{34}S$ values at Hatu is indicative of a stable homogenous fluid reservoir (Fig. 8a). The fluid oxygen fugacity constraints indicate that the ore-forming fluid at Hatu was reducing (Fan et al. 1998), and this is also suggested by the paragenesis of arsenopyrite-pyrrhotite-pyrite, and the existence of CH_4 and H_2S (Shen et al. 2016), and the absence of hematite and sulfates in the ore and wall rocks (Fig. 7). In such a situation, gold migrated as a bisulfide complex such as $Au(HS)_2^-$ or AuHS (Hayashi and Ohmoto 1991; Tomkins 2010). Because the fractionation factor of aqueous H_2S and solid sulfides was less than 1‰, the $\delta^{34}S$ values of sulfides at Hatu indicate that the sulfur in the ore-forming fluid was reduced and was from a specific source (Ohmoto and Rye 1979). Furthermore, the invariable $\delta^{34}S$ signatures in arsenopyrite and pyrite suggest that the ore-forming fluid of the Hatu gold deposit obtained sulfur from the same reservoir throughout its evolution. Integration of new and previous data indicates that sulfides in the Hatu gold mining district mainly had $\delta^{34}S$ values of −3‰–4‰, except for the Mandongshan gold deposit with low $\delta^{34}S$ values of < −3‰ (Fig. 8b). Such a remarkably uniform sulfur isotopic composition excludes the mixing of ore-forming fluids from multiple sources and points to a unique genetic process and source region. However, the low $\delta^{34}S$ values of the Mandongshan deposit do not appear to be the result of oxidation during the mineralization process such as for the Shanggong gold deposit (Chen et al. 2004b). Mineralogical and geochemical studies of the ore and wall rocks have shown that the fluid properties are characteristic of a reduced lode gold deposit (Zhang and Zhu 2017). Hence, isotope exchange during fluid-rock interaction along the pathways of the ore-forming fluid may have led to the low $\delta^{34}S$ values of the Mandongshan gold deposit.

Geochronological studies have dated the Early Carboniferous volcanic and sedimentary rocks to 357.5 ± 5.4 to 315 ± 4.0 Ma (Wang and Zhu 2007; An and Zhu 2009; Guo et al. 2010; Tang et al. 2012). A number of fossils and trace fossils have been observed in the strata, which indicate a marine facies environment (Jin and Li 1999; Gong and Zong 2015). These similar features indicate that the volcanic and sedimentary rocks may have similar origins and thus similar sulfur isotopic compositions.

Investigations in the metasedimentary and metabasaltic rocks of New Zealand and Canada have been suggested to be important source for orogenic gold deposit, confined that the gold, sulfur and arsenic are released from enrichments in sedimentary pyrite (Pitcairn et al. 2006, 2010). Thermodynamic modeling reveals that the sulfidation process of chlorite/muscovite to form pyrrhotite release water and a significant amount of Au can be liberated from the process of the pyrite to pyrrhotite transition (Zhong et al. 2015). Although framboidal pyrite, host in the carbonaceous mudstone of the Early Carboniferous volcano-sedimentary rocks, exhibits a wide range of $\delta^{34}S$ values (–26.7‰–54.0‰; An et al. 2023), the median value, at 0.9‰, is comparable to the values obtained in hydrothermal pyrite and arsenopyrite at Hatu gold deposit, ranging from − 0.8‰ to 1.3‰ (Table S1 and Fig. 8b). Thus, we interpret this similarity as the result of homogenization of sulfur during metamorphism (Chen and Zhang 1991; Groves et al. 2003; Chang et al. 2008). The near-zero $\delta^{34}S$ values observed at Hatu suggests the thorough homogenization of the original sulfur isotope during the metamorphism dehydration of the Early Carboniferous volcano-sedimentary rocks, coinciding with the release of gold and other elements.

Lead isotope, being widely accepted as an important tracer, can be utilized to interpret the material source and tectonic environment of ore formation (White et al. 2016). Pyrite and arsenopyrite in early and middle stages of the Hatu gold deposit have narrow ranges of $^{207}Pb/^{204}Pb$ (15.492–15.571, average: 15.529) and $^{208}Pb/^{204}Pb$ (37.802–38.113, average: 37.905) ratios, suggesting a common source of lead. Previously published data show that whole-rock analyses of the Early Carboniferous volcanic rocks revealed that the $^{206}Pb/^{204}Pb$, $^{207}Pb/^{204}Pb$, and $^{208}Pb/^{204}Pb$ ratios had ranges of 17.147–19.744, 15.392–15.627, and 37.628–38.838, respectively, and averages of 18.022, 15.497, and 38.137, respectively (Table S2). Feldspar analyses indicated that the Late Paleozoic granitoid rocks had $^{206}Pb/^{204}Pb$, $^{207}Pb/^{204}Pb$, and $^{208}Pb/^{204}Pb$ ratios of 17.690–18.330, 15.260–15.500, and 37.130–38.080, respectively, with averages of 18.016, 15.398, and 37.635, respectively (Table S2). The $^{207}Pb/^{204}Pb$ and $^{208}Pb/^{204}Pb$ ratios of the Late Paleozoic granitoids had quite large variations.

The $^{207}Pb/^{204}Pb$-$^{206}Pb/^{204}Pb$ diagram (Fig. 9a) showed that the sulfides fell between the evolution curves of the mantle and orogen (Zartman and Doe 1981). These results indicate that juvenile crustal material, which is widely distributed throughout West Junggar (Jahn et al. 2000), contributed variable amounts of Pb to the ore. Similarly, the $^{208}Pb/^{204}Pb$-$^{206}Pb/^{204}Pb$ diagram (Fig. 9b) plotted the ore samples across the curves of the orogen, mantle, and upper crust, and most were clustering between the curves of the lower crust and orogen (Zartman and Doe 1981). The Pb isotope data of the sulfides are notably higher than the Late Paleozoic granitoid rocks, and the latter were mainly distributed below the evolution curve of the orogen. This indicates

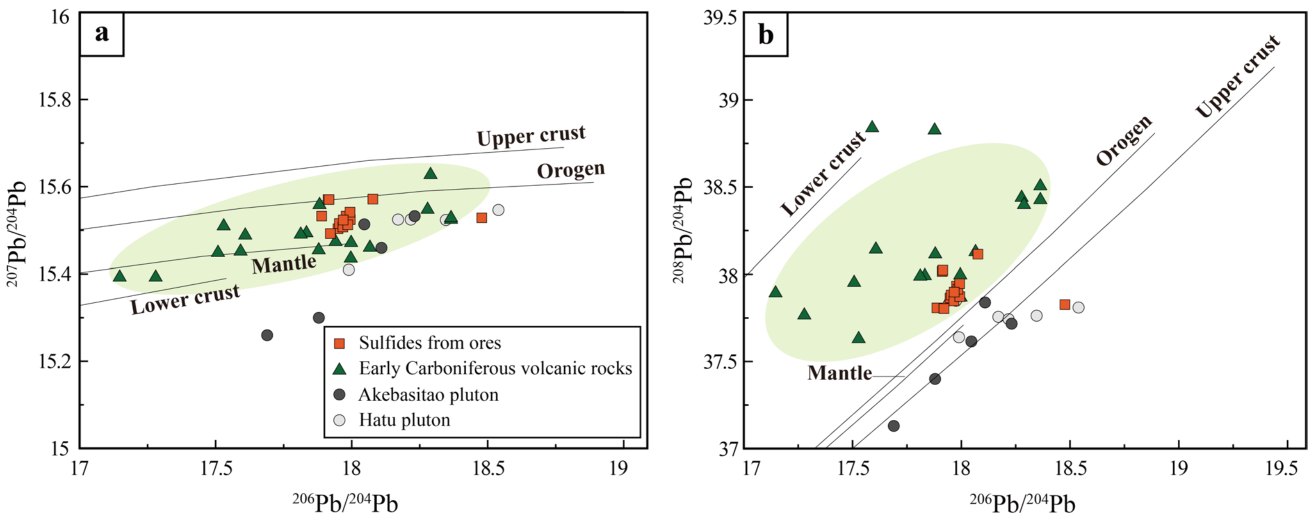

Fig. 9 Lead isotopic compositions of the Hatu gold deposit and related lithologies (base map from Zartman and Doe 1981)

that the sulfides cannot have originated from Paleozoic granitoid rocks. In particular, the $^{207}Pb/^{204}Pb$-$^{206}Pb/^{204}Pb$ and $^{208}Pb/^{204}Pb$-$^{206}Pb/^{204}Pb$ diagrams showed that the ratios for sulfides followed trends similar to those of the Early Carboniferous volcanic rocks. Therefore, it is highly probable that the Pb in sulfides originated predominantly from Early Carboniferous volcanic rocks, which possessed Pb isotopes characteristic of the lower crust and/or mantle reservoirs. Many orogenic gold deposits throughout the world have shown similar Pb isotopic compositions for the ore and wall rock. (Ho et al. 1995; Meffre et al. 2008; Mortensen et al. 2010; Aibai et al. 2021; Muhtar et al. 2021).

In summary, the S-Pb isotopic composition was remarkably similar throughout the Hatu gold deposit, which indicates that it may have originated from a large and uniform fluid and metal source reservoir. The Early Carboniferous volcanic and sedimentary rocks are a suitable candidate for the fluid and material reservoirs of the deposit.

5.2 Genetic type of the Hatu gold deposit

The West Junggar is tectonically correlated with East Kazakhstan, and recent studies have showed that the northern and central West Junggar are extensions of the Kazakhstan continent to the east (Windley et al. 2007; Chen et al. 2010, 2015; Li et al. 2022). In the Late Silurian, the southern West Junggar terrane collided with the Yili Block to constituted the Kazakhstan continent, and thereafter, the West Junggar has experienced the same tectonic processes as the Yili-Kazakhstan continental plate (Ren et al. 2018). Li et al. (2022) interpreted the P-T-t path of the collision between Yili-Kazakhstan and Siberian continental plates during the Late Carboniferous as occurring in three distinct stages, prograde (ca. 322–300 Ma), near-isothermal decompression (ca. 300 Ma) and retrograde (ca. 300–268 Ma). Furthermore, Zheng et al. (2020) divided the geodynamic evolution of West Junggar into subduction stage (ca. 572–324 Ma),

Table 1 Ages of the gold deposits formation in Hatu gold district

Deposit	Age (Ma)	Material description	Method (mineral)	References
Hatu	290 ± 5	Auriferous quartz vein	Rb–Sr (quartz)	Li et al. (2000)
Hatu	308.6 ± 4.2	Auriferous quartz vein	Ar–Ar (quartz)	Shen and Jin (1993)
Qi-II	289 ± 29	Auriferous quartz vein	Rb–Sr (quartz)	Li et al. (2000)
Qi-V	299.6 ± 1.9	Albite-quartz-muscovite vein	U–Pb (zircon)	Wang (2015)
Qi-V	300 ± 2	Gold-bearing sulfide-muscovite-carbonate-quartz vein	U–Pb (zircon)	An et al. (2024)
Qi-V	299.6 ± 1.7	Gold-bearing sulfide-muscovite-carbonate-quartz vein	Ar–Ar (muscovite)	An et al. (2024)
Qi-V	299.9 ± 1.8	Gold-bearing sulfide-muscovite-carbonate-quartz vein	Ar–Ar (muscovite)	An et al. (2024)
Qi-V	300.6 ± 1.9	Gold-bearing sulfide-muscovite-carbonate-quartz vein	Ar–Ar (muscovite)	An et al. (2024)
Huilvshan	300 ± 1.7	Quartz-ankerite-polymetallic sulfide vein	Ar–Ar (muscovite)	Zhang and Zhu (2021)
Huilvshan	301.1 ± 1.8	Quartz-ankerite-polymetallic sulfide vein	Ar–Ar (muscovite)	Zhang and Zhu (2021)

collision stage (ca. 324–318 Ma), and post-collision stage (ca. 318–263 Ma).

Previous investigations using different methodologies have indicated that the Hatu deposit formed during the Permo-Carboniferous (Table 1). Shen and Jin (1993) initially ascertained a 309 ± 4 Ma $^{40}Ar/^{39}Ar$ plateau age of the fluid inclusions within quartz. Li et al. (2000) reported a Rb–Sr isochron age from fluid inclusions in auriferous quartz of 290 ± 5 Ma; this date was interpreted as approximating the timing of alteration and mineralization. The mineralization timing and its correlation with the Late Paleozoic tectonic evolution suggest that the formation of the Hatu deposit coincided with geodynamic processes transitioning from collisional compression to extension (Chen and Zhang 1991; Zhang et al. 2013; Li et al. 2014; Wu et al. 2018; Ding et al. 2019). Additionally, the geological evidence from Hatu indicates that the early-stage veins were structurally deformed (Fig. 3f), fractured and recemented by non-deformed middle-stage stockworks (Figs. 3e, 5g). The late-stage veins are open-space fillings that crosscut earlier veins (Fig. 5k), indicating that the mineralization is associated with transitions from compressive to transitional compression-to-extension, and ultimately to extensional settings, consistent with the Late Paleozoic tectonic evolution of West Junggar. The S and Pb isotopic features indicate that the ore metals in the Hatu gold deposit originated from metamorphic processes. Previous studies show that the ore-forming fluid is characterized by low salinity (< 10 wt% NaCl equiv.) and high CO_2 content (Fan et al. 1998; Li 2016), which is similar to metamorphic fluid in origin (Chen et al. 2007). The ore-forming fluid of Hatu deposit also exhibited high $\delta^{18}O_{H2O}$ values (8.5‰–12.2‰) compared to magmatic fluid, indicating a metamorphic origin, and δD values ranging from –87‰ to –105‰ (Shen et al. 2016). The CO_2 gas extracted from the quartz fluid inclusions has $\delta^{13}C$ values ranging from –9.7‰ to –13.9‰, suggesting a carbonaceous sedimentary source like the host Tailegula Formation (Shen et al. 2016). Therefore, we propose that the Hatu gold deposit represents a typical fault-controlled lode system formed during collisional orogenesis, classified as an orogenic-type gold deposit (Goldfarb et al. 2001; Chen and Fu 1992; Chen 2006, 2013; Zhou et al. 2014b, 2022a, b, 2023; Zhang et al. 2020).

The onset of Permo-Carboniferous extensional tectonics following the collision between the Yili-Kazakhstan and Siberian continental plates signifies a tectonic regime marked by both magmatism and the development of hydrothermal gold deposits. The granite plutons surrounding the Hatu deposit, i.e. Hatu, Akebasitao, Miaoergou granites, yield zircon U-Pb ages of 305 ± 4 Ma, 290 ± 8 Ma and 309 ± 1 Ma, respectively (Han et al. 2006; Gao et al. 2014; Hu et al. 2015). The gold mineralization ages likely indicate that the Hatu deposit formed concurrently with the granitic magmatism.

The broad spatial and temporal relationship between orogenic gold deposits and these granitic plutons and their related dikes has been noted in many orogenic gold provinces throughout the world (Boorder 2012; Zhou et al. 2014a, 2015; Goldfarb et al. 2001, 2005; Taylor et al. 2022; Goldfarb and Pitcairn 2023). Orogenic gold deposits are commonly associated with a regional thermal event in convergent margins including accretionary and collisional orogens, leading to both magmatism and metamorphism, where the latter serves as the source of ore-forming fluids and metals (Groves et al. 1998; Chen et al. 2022). It is crucial to emphasize that the magma emplacement and metamorphic fluid migration may not necessarily simultaneous (Chen 2013; Goldfarb and Pitcairn 2023). Besides, geological and geochemical characteristics also illustrate a genetic connection between gold mineralization and magmatism is untenable in Hatu gold deposit. Reduced intrusion-related gold deposits, characterized by low-grade and large tonnage, typically feature ore occurrences within auriferous sheeted vein system situated in pluton cupolas (Hart and Goldfarb 2005). These deposits are genetically linked to plutons exhibiting specific geochemical characteristics, typically being metaluminous A-type granites, some of which can be alkalic (Hart 2005). However, the veins within the Hatu gold deposit are predominantly controlled by the ENE-trending Anqi fault and its subsidiary faults. The observed age relationships and consistent vein orientation strongly suggest that regional tectonic events have significantly controlled the mineralization, and no evidence of potassic alteration is evident in the Hatu gold district (Shen and Jin 1993; Zhu et al. 2013; Wang and Zhu 2015; Zheng et al. 2022).

5.3 Tectono-metallogenic model for the Hatu gold deposit

The mineralization of Hatu gold deposit is intricately linked to the brittle to brittle-ductile deformation of volcano-sedimentary rocks (Shen et al. 2016), manifesting within structurally-controlled dilational fractures (Xiao et al. 2010b). Accompanied by the evolving collisional orogenesis, the Hatu deposit underwent a three-stage hydrothermal process, aligning with the typical orogenic-type metallogenic system in the terrane scale CMF (collision, metallogenesis, and fluid) model (Chen et al. 2022). During the collision between the Yili-Kazakhstan and Siberian plates, underthrusting and metamorphic devolatilization of the Early Carboniferous volcanic and sedimentary rocks generated carbonic-rich fluids that migrated upward along shear zones and faults, precipitating the ore-forming metals upon reaching the brittle-ductile to brittle transition zone due to fracturing and pressure decreases (Fig. 10). The genetic model of gold deposits formed by collisional orogeny may facilitate

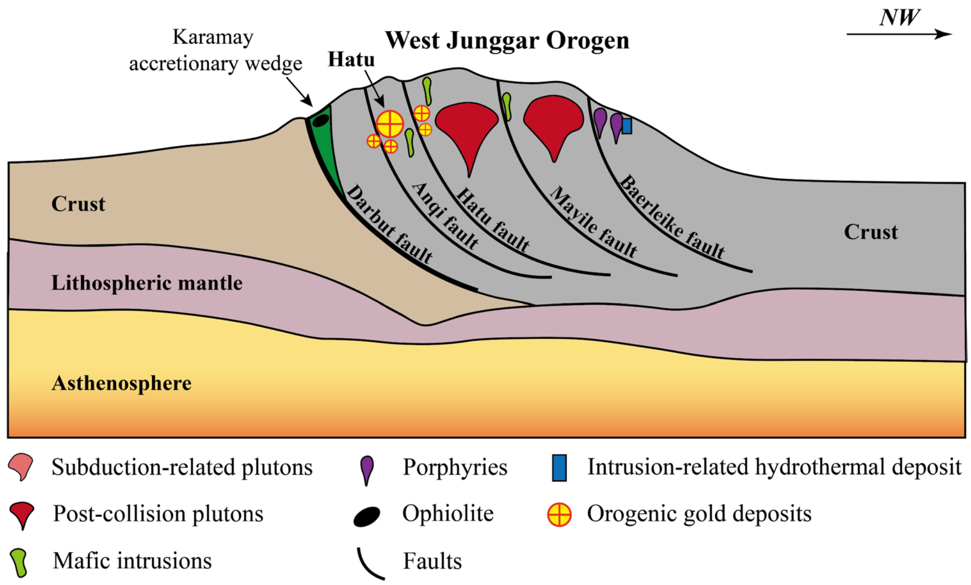

Fig. 10 The metallogenic model of Hatu gold deposit (modified after Chen 2013)

future prospecting for similar deposits or extensions of existing ones in the West Junggar.

6 Conclusion

The Hatu orogenic gold deposit is a volcano-sedimentary rock-hosted orogenic gold deposit. Ore-forming process involves the formation of early-stage pyrite-quartz-albite, middle-stage polymetallic sulfides-ankerite-quartz, and late-stage quartz-pyrite.

The sulfur isotopic values of sulfides range from − 0.8‰ to 1.3‰, averaging 0.4‰, while the lead isotopic compositions closely resemble those of the Early Carboniferous volcanic rocks, suggesting that the ore-forming metals were mainly sourced from the Early Carboniferous volcano-sedimentary rocks.

The gold mineralization in West Junggar may have resulted from the metamorphic devolatilization of the Early Carboniferous during the Permo-Carboniferous collision between the Yili-Kazakhstan and Siberian continental plates.

Acknowledgements The Western Region Gold Co., Ltd. and the geology team at the Hatu gold mine are heartly acknowledged for providing help and access to samples and information used in this study. Discussion with Dr. Rongzhen Tang helpfully improved the manuscript. We also thank Jiaxin Ding for her assistance with isotope analysis. We thank editor and an anonymous reviewer for their insightful comments and detailed reviews, which improved the quality of this manuscript.

Author contributions This study was conceptualized by Shen Han, Zhenju Zhou and Yanjing Chen. Field investigation was carried out by Shen Han, Xiaohua Deng, and Yong Wang. Shen Han, Zhenju Zhou and Yanjing Chen interpreted the data and wrote the manuscript, with contributions from all other authors.

Funding This study was supported by the National Natural Science Foundation of China (Nos. 42172093, 42202075, and 42302108), the Key Research and Development Project of Xinjiang (No. 2023B03015), the Uygur Autonomous Region Tianchi Talent Project, and the Natural Science Foundation of Xinjiang (No. 2022D01A344) and China Scholarship Council (202304180004).

References

Aibai A, Deng XH, Pirajno F, Han S, Liu WX, Li X, Chen X, Wu YS, Liu JF, Chen YJ (2021) Origin of ore-forming fluids of Tokuzbay gold deposit in the South Altai, northwest China: Constraints from Sr–Nd–Pb isotopes. Ore Geol Rev 134:104165.

An F, Zhu YF (2009) SHRIMP U-Pb zircon ages of tuff in Baogutu formation and their geological significances. Acta Petrol Sin 25:1437–1445 (**in Chinese with English abstract**).

An F, Zhu YF, Wang XW, Li YX, Qiang JL (2023) Genesis of the Hatu gold deposit: Constrained by in situ S Pb isotope geochemistry of pyrite. J Geochem Explor 254:107296.

An F, Qiu T, Zhang HC, Yuan H, Zhu YF (2024) New precise age constraints of the Hatu gold belt, west Junggar, NW China: implications for a 300 Ma magmatic hydrothermal event in post-collisional setting. Geol Soc Am Bull. https://doi.org/10.1130/B37148.1.

Boorder H (2012) Spatial and temporal distribution of the orogenic gold deposits in the Late Palaeozoic Variscides and Southern Tianshan: How orogenic are they? Ore Geol Rev 46:1–31.

Buckman S, Aitchison JC (2004) Tectonic evolution of palaeozoic terranes in West Junggar, Xinjiang, NW China. Geol Soc Lond Spec Publ 226:101–129.

Chang ZS, Large RR, Maslennikov V (2008) Sulfur isotopes in sediment-hosted orogenic gold deposits: evidence for an early timing and a seawater sulfur source. Geology 36:971–974.

Chen YJ (1996) Mineralization during collisional orogenesis and its control of the distribution of gold deposits in Junggar Mountains, Xinjiang, China. Acta Geol Sin 70:253–261 (**in Chinese with English abstract**).

Chen YJ (2006) Orogenic-type deposits and their metallogenic model and exploration potential. Geol China 33:1181–1196 (**in Chinese with English abstract**).

Chen YJ (2013) The development of continental collision metallogeny and its application. Acta Petrol Sin 29: 1–17 (**in Chinese with English abstract**).

Chen YJ, Fu SG (1992) Gold mineralization in West Henan, China. Seismological Press, Beijing, pp 234 (**in Chinese with English abstract**).

Chen YJ, Zhang CN (1991) The mineralization model for gold deposits in the Western Junggar area. J Changchun Univ Earth Sci 21:61–82 (**in Chinese with English abstract**).

Chen YJ, Pirajno F, Sui YH (2004a) Isotope geochemistry of the Tieluping silver-lead deposit, Henan, China: A case study of orogenic silver-dominated deposits and related tectonic setting. Miner. Depos. 39:560–575.

Chen YJ, Li J, Pirajno F, Lin ZJ, Wang HH (2004b) Hydrothermal metallogeny of the Shanggong gold deposit, East Qinling studies on ore geology and fluid inclusion geochemistry. J Miner Petrol 24:1–12 (**in Chinese with English abstract**).

Chen YJ, Ni P, Fan HR, Pirajno F, Su WC, Zhang H (2007) Diagnostic fluid inclusions of different types hydrothermal gold deposits. Acta Petrol Sin 23:2085–2108 (**in Chinese with English abstract**).

Chen YJ, Pirajno F, Wu G, Qi JP, Xiong XL (2012a) Epithermal deposits in north Xinjiang, NW China. Int J Earth Sci 101:889–917.

Chen YJ, Pirajno F, Li N, Deng XH, Yang YF (2022) Geology and geochemistry of molybdenum deposits in the Qinling Orogen, PR China. Springer, Singapore, pp 118–120.

Chen B, Jahn BM (2004) Genesis of post-collisional granitoids and basement nature of the Junggar Terrane, NW China: Nd–Sr isotope and trace element evidence. J Asian Earth Sci 23:691–703.

Chen JF, Han BF, Ji JQ, Zhang L, Xu Z, He GQ, Wang T (2010) Zircon U-Pb ages and tectonic implications of paleozoic plutons in northern West Junggar, North Xinjiang, China. Lithos 115:137–152.

Chen XH, Yang N, Ye BY, Wang ZH, Chen ZL (2011) Tectonic system and its control on metallogenesis in western Junggar as part of the central asia multi-core metallogenic system. Geotecton Metallog 35:325–338 (**in Chinese with English abstract**).

Chen HY, Chen YJ, Baker MJ (2012b) Isotopic geochemistry of the Sawayaerdun orogenic-type gold deposit, Tianshan, northwest China: implications for ore genesis and mineral exploration. Chem Geol 310:1–11.

Chen JF, Han BF, Zhang L, Xu Z, Liu JL, Qu WJ, Li C, Yang JH, Yang YH (2015) Middle paleozoic initial amalgamation and crustal growth in the West Junggar (NW China): Constraints from geochronology, geochemistry and Sr–Nd–Hf–Os isotopes of calc-alkaline and alkaline intrusions in the Xiemisitai-Saier Mountains. J Asian Earth Sci 113:90–109.

Chen JF, Ma X, Simon A, Du HY, Han BF, Liu JL, Liu B (2019) Late Ordovician to early Silurian calc-alkaline magmatism in the Xiemisitai mountains, northern West Junggar: A response to the subduction of the Junggar–Balkhash Ocean. Int Geol Rev 61:2000–2020.

Choulet F, Chen Y, Wang, B, Faure M, Cluzel D, Charvet J, Lin W, Xu B (2011) Late Paleozoic paleogeographic reconstruction of Western Central Asia based upon paleomagnetic data and its geodynamic implications. J Asian Earth Sci 42: 867–884.

Choulet F, Faure M, Cluzel D, Chen Y, Lin W, Wang B, Jahn BM (2012) Architecture and Evolution of Accretionary Orogens in the Altaids Collage: The Early Paleozoic West Junggar (NW China). Am J Sci 312: 1098–1145.

Coleman RG (1989) Continental growth of northwest China. Tectonics 8:621–635.

Ding JX, Han S, Huang PC, Wu YS, Zhang B, Xiao F, Wang Y (2019) The orogenic gold deposits in Western Junggar, NW China, geochronological framework, spatial distribution and tectonic implication. Geol Rev 65:1439–1461 (**in Chinese with English abstract**).

Fan HR, Jin CW, Shen YC (1998) Ore-forming fluid geochemistry of the Hatu gold deposit in Xinjiang, northwest China. Miner Depos 17:135–149 (**in Chinese with English abstract**).

Feng Y, Coleman RG, Tilton GR, Xiao X (1989) Tectonic evolution of the west Junggar region, Xinjiang, China. Tectonics 8:729–752.

Filippova IB, Bush VA, Didenko AN (2002) Middle paleozoic subduction belts: the leading factor in the formation of the Central Asian fold- and-thrust belt. Russ J Earth Sci 3:405–426.

Gao R, Xiao L, Pirajno F, Wang GC, He XX, Yang G, Yan SW (2014) Carboniferous-Permian extensive magmatism in the West Junggar, Xinjiang, northwestern China: Its geochemistry, geochronology, and petrogenesis. Lithos 204:125–143.

Goldfarb RJ, Pitcairn I (2023) Orogenic gold: Is a genetic association with magmatism realistic? Miner Depos 58:5–35.

Goldfarb RJ, Newberry RJ, Pickthorn WJ, Gent CA (1991) Oxygen, hydrogen, and sulfur isotope studies in the Juneau gold belt, southeastern Alaska; constraints on the origin of hydrothermal fluids. Econ Geol 86:66–80.

Goldfarb RJ, Groves DI, Gardoll S (2001) Orogenic gold and geologic time: A global synthesis. Ore Geol Rev. 18:1–75.

Goldfarb RJ, Baker T, Dubé B, Groves DI, Hart CJR, Gosselin P (2005) Distribution, character, and genesis of gold deposits in metamorphic terranes. Econ Geol 100th Anniv Vol, pp 407–450.

Gong YM, Zong RW (2015) Paleozoic stratigrahic regionalization and Paleogeograhic evolution in Western Junggar, Northwestern China. Earth Sci J China Univ Geosci 40:461–484 (**in Chinese with English abstract**).

Groves DI, Goldfarb RJ, Gebre-Mariam M, Hagemann SG, Robert F (1998) Orogenic gold deposits: a proposed classification in the context of their crustal distribution and relationship to other gold deposit types. Ore Geol Rev. 13:7–27.

Groves DI, Goldfarb RJ, Robert F, Hart CJ (2003) Gold deposits in metamorphic belts: Overview of current understanding, outstanding problems, future research, and exploration significance. Econ Geol 98:1–29.

Guo LS, Liu YL, Wang ZH, Song D, Xu FJ, Su L (2010) The zircon U-Pb LA-ICP-MS geochronology of volcanic rocks in Baogutu areas, western Junggar. Acta Petrol Sin 26:471–477 (**in Chinese with English abstract**).

Han BF, Wang SG, Jahn BM, Hong DW, Kagami H, Sun YL (1997) Depleted-mantle source for the Ulungur River A-type granites from North Xinjiang, China: Geochemistry and Nd–Sr isotopic evidence, and implications for Phanerozoic crustal growth. Chem Geol 138:135–159.

Han BF, Ji JQ, Song B, Chen LH, Zhang L (2006) Late Paleozoic vertical growth of continental crust around the Junggar Basin, Xinjiang, China (Part I): Timing of post-collisional plutonism. Acta Petrol Sin 22:1077–1086 (**in Chinese with English abstract**).

Hart CJR (2005) Classifying, distinguishing and exploring for intrusion-related gold systems. Gangue 87(1):4–9.

Hart CJR, Goldfarb RJ (2005) Distinguishing intrusion-related from orogenic gold systems. In: New Zealand minerals conference proceedings. Australasian Institute of Mining and Metallurgy, pp 125–133.

Hayashi K, Ohmoto H (1991) Solubility of gold in NaCl- and H_2S-bearing aqueous solutions at 250–350 °C. Geochim Cosmochim Acta 55:2111–2126.

Ho SE, McQueen KG, McNaughton NJ, Groves DI (1995) Lead isotope systematics and pyrite trace element geochemistry of two granitoid-associated mesothermal gold deposits in the southeastern Lachlan fold belt. Econ Geol 90:1818–1830.

Hodkiewicz PF, Groves DI, Davidson GJ, Weinberg RF, Hagemann SG (2009) Influence of structural setting on sulphur isotopes in

Archean orogenic gold deposits, Eastern Goldfields Province, Yilgarn, Western Australia. Miner Depos 44:129–150.
Hong Y, Liu B (2021) Tracking the tectonic evolution of the Junggar–Balkhash ocean: A case study from the post-collisional Takergan Pluton in the West Junggar, Xinjiang. J Earth Sci 32:1250–1261.
Hu Y, Wang JL, Wang JQ, Yang M, Yuan P, Ling WW (2015) Geochemistry and geochronology of the Miaoergou granite pluton in West Junggar, Xinjiang. Acta Geol Sin 31:505–522 (**in Chinese with English abstract**).
Huang PH (2015) Petrology and geochemistry of late Paleozoic granitoids in the West Junggar Metallogenic Belt (Xinjiang), Central Asia, and tectonic implications. Master Dissertation. Beijing. China University of Geosciences (Beijing), pp 49–69 (**in Chinese with English abstract**).
Jahn BM, Wu FY, Chen B (2000) Granitoids of the Central Asian Orogenic Belt and continental growth in the Phanerozoic. Trans R Soc Edinb Earth Sci. 91:181–193.
Jia YF, Li X, Kerrich R (2001) Stable isotope (O, H, S, C, and N) systematics of quartz vein systems in the turbidite-hosted Central and North Deborah gold deposits of the Bendigo gold field, central Victoria, Australia: Constraints on the origin of ore-forming fluids. Econ Geol 96:705–721.
Jin HJ, Li YC (1999) Carboniferous biogenic sedimentary structures on the northwestern margin of Jungar Basin. Chin Sci Bull 44:368–372.
Kishida A, Kerrich R (1987) Hydrothermal alteration zoning and gold concentration at the Kerr–Addison Archean lode gold deposit, Kirkland Lake, Ontario. Econ Geol 82:649–690.
Khain EV, Bibikova EV, Kröner A, Zhuravlev DZ, Sklyarov EV, Fedotova AA, Kravchenko-Berezhnoy IR (2002) The most ancient ophiolite of the Central Asian fold belt: U–Pb and Pb–Pb zircon ages for the Dunzhugur Complex, Eastern Sayan, Siberia, and geodynamic implications. Earth Planet Sci Lett 199: 311–325.
Kovalenko VI, Yarmolyuk VV, Kovach VP, Kotov AB, Kozakov IK, Salnikova EB, Larin AM (2004) Isotope provinces, mechanisms of generation and sources of the continental crust in the Central Asian mobile belt: geological and isotopic evidence. J Asian Earth Sci 23:605–627.
Kröner A, Windley BF, Badarch G, Tomurtogoo O, Hegner E, Jahn BM, Gruschka S, Khain EV, Demoux A, Wingate MTD (2007) Accretionary growth and crust formation in the Central Asian Orogenic Belt and comparison with the Arabian-Nubian shield. Memoirs-Geological Society of America 200: 181–209.
Kröner A, Kovach V, Belousova E, Hegner E, Armstrong R, Dolgopolova A, Seltmann R, Alexeiev DV, Hoffmann JE, Wong J (2014) Reassessment of continental growth during the accretionary history of the Central Asian Orogenic Belt. Gondwana Res 25:103–125.
LaFlamme C, Sugiono D, Thébaud N, Caruso S, Fiorentini M, Selvaraja V, Jeon H, Voute F, Martin L (2018) Multiple sulfur isotopes monitor fluid evolution of an Archean orogenic gold deposit. Geochim Cosmochim Acta 222:436–446.
Li HQ, Chen FW, Cai H (2000) Study on Rb–Sr isotopic ages of gold deposits in West Junggar area, Xinjiang. Acta Geol Sin 74:181–192 (**in Chinese with English abstract**).
Li D, He DF, Yang YH, Lian YC (2014) Petrogenesis of mid-Carboniferous volcanics and granitic intrusions from western Junggar Basin boreholes: geodynamic implications for the Central Asian Orogenic Belt in Northwest China. Int Geol Rev 56:1668–1690.
Li JY, Chen XH, Ding WC, Wang ZH, Chen W, Li B, Huang PH (2016) $^{40}Ar/^{39}Ar$ Thermochronology of late paleozoic granitoids in West Junggar (Xinjiang, China). Central Asia Geotecton Metallog 40:386–404 (**in Chinese with English abstract**).
Li D, He DF, Lian YC, Lu Y, Yi ZJ (2017) Structural evolution and late carboniferous magmatism of the zhongguai arc in the western Junggar Basin, Northwest China: implications for tectonic evolution of the Junggar Ocean. Int Geol Rev 59:1234–1255.
Li A, Xu Y, Liao W, Han BF, Wei C (2022) High-pressure granulite-facies metamorphism in the junction between the Siberian and Kazakhstan–Junggar continents and implications for the assembly of Pangea. Gondwana Res 110:13–30.
Li J (2016) Geochemical characteristics of ore-forming fluid from Hatu gold metalogeny. Master dissertation. North China University of Science and Technology, Tangshan, pp 1–69 (**in Chinese with English abstract**).
Liao W, Han BF, Xu Y, Li A (2021) Ediacaran initial subduction and Cambrian slab rollback of the Junggar Ocean: new evidence from igneous tectonic blocks and gabbro enclave in Early Palaeozoic accretionary complexes, southern West Junggar, NW China. Geol Mag 158:1811–1829.
Lin W, Sun P, Xue ZH, Zhang ZP (2017) Structural analysis of late paleozoic deformation of central dalabute fault zone, West Junggar, China. Acta Geol Sin 33:2987–3001 (**in Chinese with English abstract**).
Liu B, Chen JF, Ma X, Liu JL, Gong EP, Shi WG, Han BF (2018) Timing of the final closure of the Irtysh–Zaysan Ocean: New insights from the earliest stitching pluton in the northern West Junggar, NW China. Geol J 53:2810–2823.
Liu Y, Wang X, Wu KY, Chen SN, Shi Z, Yao WJ (2019) Late Carboniferous seismic and volcanic record in the northwestern margin of the Junggar Basin: Implication for the tectonic setting of the West Junggar. Gondwana Res 71:49–75.
Meffre S, Large RR, Scott R, Woodhead J, Chang Z, Gilbert SE, Danyushevsky LV, Maslennikov V, Hergt JM (2008) Age and pyrite Pb-isotopic composition of the giant Sukhoi Log sediment-hosted gold deposit, Russia. Geochim Cosmochim Acta 72:2377–2391.
Mortensen JK, Craw D, MacKenzie DJ, Gabites JE, Ullrich T (2010) Age and origin of orogenic gold mineralization in the otago schist belt, south island, New Zealand: Constraints from lead isotope and $^{40}Ar/^{39}Ar$ dating studies. Econ Geol 105:777–793.
Muhtar MN, Wu CZ, Brzozowski MJ, Lei RX, Feng ZJ, Chen BY, Jiang YH (2021) Sericite $^{40}Ar/^{39}Ar$ dating and S-Pb isotope composition of the Kanggur gold deposit: Implications for metallogenesis of late Paleozoic gold deposits in the Tianshan, central Asian Orogenic Belt. Ore Geol Rev 131:104056.
Ohmoto H (1972) Systematics of sulfur and carbon isotopes in hydrothermal ore deposits. Econ Geol 67:551–578.
Ohmoto H, Rye RO (1979) Isotopes of sulfur and carbon. In: Barnes HL (ed) Geochemistry of Hydrothermal ore deposits. Wiley, New York, pp 509–567.
Phillips GN, Powell R (2010) Formation of gold deposits: a metamorphic devolatilization model. J Metamorph Geol 28: 689–718.
Pirajno F, Seltmann R, Yang Y (2011) A review of mineral systems and associated tectonic settings of northern Xinjiang, NW China. Geosci Front 2:157–185.
Pitcairn IK, Teagle DA, Craw D, Olivo GR, Kerrich R, Brewer TS (2006) Sources of metals and fluids in orogenic gold deposits: Insights from the Otago and Alpine Schists, New Zealand. Econ Geol 101:1525–1546.
Pitcairn IK, Olivo GR, Teagle DA, Craw D (2010) Sulfide evolution during prograde metamorphism of the Otago and Alpine Schists, New Zealand. Canad Miner 48:1267–1295.
Ren R, Han BF, Xu Z, Zhou YZ, Liu B, Zhang L, Chen JF, Su L, Li J, Li XH, Li QL (2014) When did the subduction first initiate in the southern Paleo-Asian Ocean: New constraints from a Cambrian intra-oceanic arc system in West Junggar, NW China. Earth Planet Sci Lett 388:222–236.
Ren R, Han BF, Guan SW, Liu B, Wang ZZ (2018) Linking the southern West Junggar terrane to the Yili Block: Insights from the

oldest accretionary complexes in West Junggar, NW China. J Asian Earth Sci 159:279–293.

Richards JP, Kerrich R (1993) The Porgera gold mine, Papua New Guinea; magmatic hydrothermal to epithermal evolution of an alkalic-type precious metal deposit. Econ Geol 88:1017–1052.

Seal RR (2006) Sulfur isotope geochemistry of sulfide minerals. Rev Miner Geochem 61:633–677.

Şengör AMC, Natal'In BA (1996) Turkic-type orogeny and its role in the making of the continental crust. Annu Rev Earth Planet Sci 24:263–337.

Şengör AMC, Natal'In BA, Burtman VS (1993) Evolution of the Altaid tectonic collage and Palaeozoic crustal growth in Eurasia. Nature 364:299–307.

Shen YC, Jin CW (1993) Magmatism and gold mineralization in West Junggar. Science Press, Beijing, pp 1–239 (**in Chinese with English abstract**).

Shen P, Shen YC, Pan CZ, Pan HD, Dai HW, Meng L (2010) Zircon age and metallogenic characteristics of the Hatu-Baogutu Au–Cu metallogenic concentric region in Xinjiang. Acta Petrol Sin 26:2879–2893 (**in Chinese with English abstract**).

Shen P, Pan HD, Zhu HP (2016) Two fluid sources and genetic implications for the Hatu gold deposit, Xinjiang, China. Ore Geol Rev 73:298–312.

Tang GJ, Wang Q, Wyman DA, Li ZX, Zhao ZH, Yang YH (2012) Late Carboniferous high $\varepsilon_{Nd}(t)$-$\varepsilon_{Hf}(t)$ granitoids, enclaves and dikes in Western Junggar, NW China: Ridge-subduction-related magmatism and crustal growth. Lithos 140:86–102.

Taylor RD, Morgan LE, Jourdan F, Monecke T, Marsh EE, Goldfarb RJ (2022) Late Jurassic-Early Cretaceous orogenic gold mineralization in the Klamath Mountains, California: constraints from $^{40}Ar/^{39}Ar$ dating of hydrothermal muscovite. Ore Geol Rev 141:104661.

Tomkins AG (2010) Windows of metamorphic sulfur liberation in the crust: Implications for gold deposit genesis. Geochim Cosmochim Acta 74:3246–3259.

Wang R, Zhu YF (2007) Geology of the Baobei gold deposit in Western Junggar and zircon SHRIMP age of its wall-rocks, western Junggar (Xinjiang, NW China). Geol J China Univ 13:590–602 (**in Chinese with English abstract**).

Wang L, Zhu YF (2015) Multi-stage pyrite and hydrothermal mineral assemblage of the Hatu gold district (West Junggar, Xinjiang, NW China): Implications for metallogenic evolution. Ore Geol Rev 69:243–267.

Wang RK, Maimaiti D, Wu ZN, Eresi K, Bai XY, Wang JL, Wang Y, Liu B, Lin CX (2019a) Analysis of ore-forming fluid composition and isotope geochemical characteristics of Hatu gold mine in Xinjiang. Nonferrous Met Eng 9:77–84 (**in Chinese with English abstract**).

Wang RK, Maimaiti D, Wang Y, Wang JL, Liu B, Lin CX, Eresi K, Bai YX (2019b) Physicochemical characteristics of fluid inclusions and mineralization significance of Hatu gold deposit, Xinjiang. Acta Miner Sin 39:83–91 (**in Chinese with English abstract**).

Wang L (2015) Study of hydrothermal gold mineralization in Hatu Qi-V ore region in western Junggar, Xinjiang (NW China). Doctor Dissertation. Peking University, Beijing, pp 49–57 (**in Chinese with English abstract**).

Weng K, Ma ZP, Cao K, Dong YP, Chen B, Zhao XJ (2020) Petrogenesis and tectonic implications of the Early Carboniferous volcanic rocks in West Junggar, NW China. Geol J 55:1826–1848.

Western Region Gold Karamay Hatu Gold Deposit (WRGKHGD) Co., Ltd (2018) Verification report of gold resources and reserves in Qi-I mining area of Hatu gold mine in Tuoli, Xinjiang.

White LF, Bailey I, Foster GL, Allen G, Kelley SP, Andrews JT, Hogan K, Dowdeswell JA, Storey CD (2016) Tracking the provenance of Greenland-sourced, Holocene aged, individual sand-sized ice-rafted debris using the Pb-isotope compositions of feldspars and $^{40}Ar/^{39}Ar$ ages of hornblendes. Earth Planet Sci Lett 433:192–203.

Windley BF, Alexeiev D, Xiao WJ, Kroner A, Badarch G (2007) Tectonic models for accretion of the Central Asian Orogenic Belt. J Geol Soc 164:31–47.

Wu C, Hong T, Xu XW, Cao MJ, Li H, Zhang GL, You J, Ke Q, Dong LH (2018) Tectonic evolution of the Paleozoic Barluk continental arc, West Junggar, NW China. J Asian Earth Sci 160:48–66.

Xiao WJ, Windley BF, Hao J, Zhai MG (2003) Accretion leading to collision and the Permian Solonker suture, Inner Mongolia, China: Termination of the central Asian orogenic belt. Tectonics 22:1069.

Xiao WJ, Han CM, Yuan C, Sun M, Lin SF, Chen HL, Li ZL, Li JL, Sun S (2008) Middle Cambrian to Permian subduction-related accretionary orogenesis of Northern Xinjiang, NW China: Implications for the tectonic evolution of central Asia. J Asian Earth Sci 32:102–117.

Xiao WJ, Kusky T (2009) Geodynamic processes and metallogenesis of the Central Asian and related orogenic belts: Introduction. Gondwana Res 16: 167–169.

Xiao WJ, Huang BC, Han CM, Sun S, Li JL (2010a) A review of the western part of the Altaids: A key to understanding the architecture of accretionary orogens. Gondwana Res 18:253–273.

Xiao F, Xu CY, Zhang FJ, Lin CX (2010b) Major breakthrough in the Hatu gold deposit, Western Junggar, Xinjiang. Xinjiang Geol 28:409–412 (**in Chinese with English abstract**).

Xu Z, Han BF, Ren R, Zhou YZ, Zhang L, Chen JF, Su L, Li XH, Liu DY (2012) Ultramafic-mafic melange, island arc and post-collisional intrusions in the Mayile Mountain, West Junggar, China: Implications for Paleozoic intra-oceanic subduction-accretion process. Lithos 132:141–161.

Xu Z, Han BF, Ren R, Zhou YZ, Su L (2013) Palaeozoic multiphase magmatism at Barleik Mountain, southern West Junggar, Northwest China: Implications for tectonic evolution of the West Junggar. Int Geol Rev 55:633–656.

Yang GX, Li YJ, Gu PY, Yang BK, Tong LL, Zhang HW (2012) Geochronological and geochemical study of the Darbut Ophiolitic Complex in the West Junggar (NW China): Implications for petrogenesis and tectonic evolution. Gondwana Res 21:1037–1049.

Yang GX, Li YJ, Yan J, Tong LL, Han X, Wang YB (2014) Geochronological and geochemical constraints on the origin of the 304 ± 5 Ma Karamay A-type granites from West Junggar, Northwest China: Implications for understanding the Central Asian Orogenic Belt. Int Geol Rev 56:393–407.

Yang Y, Zhao L, Zheng R, Xu Q, Liu J, Zhang J (2020) An Early Ordovician fossil seamount of the Hongguleleng-Balkybey Ocean in the northern West Junggar terrane (NW China) and its implications for the ocean evolution. J Asian Earth Sci 194:104066.

Zartman RE, Doe BR (1981) Plumbotectonics—the model. Tectonophysics 75:135–162.

Zhang FJ (2003) Discussions on the ore bearing structure of the associated minerals and the geology of mineral veins in Xinjiang Hatu gold ore. Xinjiang Nonferrous Metals 3:5–6 (**in Chinese with English abstract**).

Zhang HC, Zhu YF (2017) Genesis of the Mandongshan gold deposit (Xinjiang, NW China): T-P-fS_2 and phase equilibria constraints from the Au–As–Fe–S system. Ore Geol Rev 83:135–151.

Zhang HC, Zhu YF (2021) Textural, trace elemental and sulfur isotopic signatures of arsenopyrite and pyrite from the Mandongshan gold deposit (west Junggar, NW China): Implications for the conditions of gold mineralization. Ore Geol Rev 129:103938.

Zhang Y, Pe-Piper G, Piper DJW, Guo Z (2013) Early Carboniferous collision of the Kalamaili orogenic belt, North Xinjiang, and its implications: Evidence from molasse deposits. Geol Soc Am Bull 125:932–944.

Zhang T, Chen ZL, Huang HY, Zhang WG, Zhang Q, Pan JY, Zhou ZJ, Zou ML, Feng HY, Wang XH, Han FB, Sun Y, Huo HL, Ma J, Yang B (2020) Geochemical characteristics of gold-bearing minerals and its geological significance in the Ashawayi gold deposit in the southwestern Tianshan Orogen. J Geomech 26(3):443–458 (**in Chinese with English abstract**).

Zheng JP, Sun M, Zhao GC, Robinson PT, Wang FZ (2007) Elemental and Sr–Nd–Pb isotopic geochemistry of Late Paleozoic volcanic rocks beneath the Junggar basin, NW China: Implications for the formation and evolution of the basin basement. J Asian Earth Sci 29:778–794.

Zheng B, Han BF, Liu B, Wang ZZ (2019) Ediacaran to Paleozoic magmatism in West Junggar Orogenic Belt, NW China, and implications for evolution of Central Asian Orogenic Belt. Lithos 338:111–127.

Zheng B, Han BF, Wang ZZ, Liu B, Feng LX (2020) An example of Phanerozoic continental crustal growth: The West Junggar Orogenic Belt, Northwest China. Lithos 376–377:105745.

Zheng JH, Shen P, Feng WY (2022) Hydrothermal apatite record of ore-forming processes in the Hatu orogenic gold deposit, West Junggar, Northwest China. Contrib Mineral Petrol 177:1–17.

Zhi Q, Li YJ, Duan FH, Chen J, Gao JB, Tong LL (2021) Geochronology and geochemistry of Early Carboniferous basalts from Baogutu Formation in West Junggar, Northwest China: evidence for a back-arc extension. Int Geol Rev 63:1521–1539.

Zhong RC, Brugger J, Tomkins AG, Chen YJ, Li WB (2015) Fate of gold and base metals during metamorphic evolatilization of a pelite. Geochim Cosmochim Acta 171:338–352.

Zhou ZJ, Chen YJ, Jiang SY, Zhao HX, Qin Y, Hu CJ (2014a) Geology, geochemistry and ore genesis of the Wenyu gold deposit, Xiaoqinling gold field, southern margin of North China Craton. Ore Geol Rev 59:1–20.

Zhou ZJ, Liu ZW, Qin Y (2014b) Geology, geochemistry and genesis of the Huachanggou gold deposit, western Qinling Orogen, central China. Geol J 49:424–441.

Zhou ZJ, Chen YJ, Jiang SY, Hu CJ, Qin Y, Zhao HX (2015) Isotope and fluid inclusion geochemistry and ore genesis of the Qiangma gold deposit, Xiaoqinling gold field, Qinling Orogen, southern margin of North China Craton. Ore Geol Rev 66:47–64.

Zhou ZJ, Chen ZL, Zhang WG, Huo HL, Liu B, Yan QJ, Li JL (2022a) Geology, C–H–O isotopes, and muscovite ^{40}Ar-^{39}Ar dating of the Qingbaishan gold deposit: implications for tectonism and metallogenesis of early Devonian gold deposits in the Beishan orogeny, NW China. Ore Geol Rev 145:104895.

Zhou ZJ, Chen ZL, Zhang WG, Zhang T, Zhang Q, Han FB, Huo HL, Yang B, Ma J, Wang W, Wang C, Liu XJ (2022b) Structural deformation and fluid evolution associated with the formation of the Sawayardun gold deposit in Southwestern Tianshan Orogen. Geol China 49(1):181–200 (**in Chinese with English abstract**).

Zhou ZJ, Chen ZL, Stefan W, Ingo H, Huo HL, Zhang WG, Li N, Zhang Q, Han FB, Feng HY (2023) Metal source and ore precipitation mechanism of the Ashawayi orogenic gold deposit, Southwestern Tianshan Orogen, Western China: Constraints from textures and trace elements in pyrite. Ore Geol Rev 157:105452.

Zhu YF, An F, Xu CY, Guo HT, Xia F, Xiao F, Zhang FJ, Lin CX, Qiu T, Wei SN (2013) Geology and Au–Cu deposits in the Hatu and its adjacent region (Xinjiang): Evolution and prospective model. Geological Publishing House, Beijing, pp 1–161 (**in Chinese with English abstract**).